Journal of Microscopy, Vol. 229, Pt 2 2008, pp. 344–353
Received 13 November 2006; accepted 8 May 2007

Near-field–induced tunability of surface plasmon polaritons in composite metallic nanostructures

A. CHRIST*, G. LÉVÊQUE*, O. J. F. MARTIN*,
T. ZENTGRAF†, J. KUHL†, C. BAUER‡, H. GIESSEN‡
& S. G. TIKHODEEV§
**Nanophotonics and Metrology Laboratory, Swiss Federal Institute of Technology Lausanne, EPFL-STI-NAM, ELG Station 11, CH-1015 Lausanne, Switzerland*
†Max Planck Institute for Solid State Research, 70569 Stuttgart, Germany
‡4th Physics Institute, University of Stuttgart, 70550 Stuttgart, Germany
§A. M. Prokhorov General Physics Institute RAS, 119991 Moscow, Russia

Key words. Interaction, magnetic activity, near-fields, surface plasmon polaritons.

Summary

We numerically study near-field–induced coupling effects in metal nanowire-based composite nanostructures. Our multi-layer system is composed of individual gold nanowires supporting localized particle plasmons at optical wavelengths, and a spatially separated homogeneous silver slab supporting delocalized surface plasmons. We show that the localized plasmon modes of the composite structure, forming so-called magnetic atoms, can be controlled over a large spectral range by changing the thickness of the nearby metal slab. The optical response of single-wire and array-based metallic structures are compared. Spectral shifts due to wire–mirror interaction as well as the coupling between localized and delocalized surface plasmon modes in a magnetic photonic crystal are demonstrated. The presented effects are important for the optimization of metal-based nanodevices and may lead to the realization of metamaterials with novel plasmonic functionalities.

Introduction

Metal structures supporting surface plasmon polariton modes play a crucial role in several emerging fields of nanoscience, where their remarkable optical properties are currently the subject of considerable research efforts. In particular, metal nanoparticles supporting localized surface plasmon polariton modes (i.e. so-called particle plasmons) are characterized by a significant enhancement of their local electromagnetic fields (Kottmann *et al.*, 2001a, and references therein). The achievable high field intensities are a direct consequence of the excitation of collective electron charge density oscillations in the metal particles. Such plasmonic resonances allow for confining light on the nanoscale and can be applied to alter light–matter interactions. Plasmon functionalities are used for the enhancement of Raman scattering signals on surfaces (Moskovits, 1985), for the design of chemical and biological sensors (Homola *et al.*, 1999), and for the realization of novel resonant magnetic nanostructures (Linden *et al.*, 2004; Rockstuhl *et al.*, 2006). In addition to single-particle phenomena, interacting particle ensembles also exhibit interesting optical effects (Rechenberger *et al.*, 2003; Maier, 2002). A very impressive example is the use of coupled metal nanoparticles to design nanometer-scale dipole antennas. It has been demonstrated recently that direct optical excitation results in white-light supercontinuum generation due to the achievable strong field enhancement within the feed-gap of the nanoantenna (Mühlschlegel *et al.*, 2005).

Generally, all surface plasmon polariton-related phenomena such as supercontinuum generation are resonant effects and very sensitive to the chosen light frequency. Therefore, the nanoantenna design has to fulfill two fundamental requirements. First, the particle geometry and the supported collective surface plasmon polaritons should allow for a reasonably strong field enhancement. Second, the plasmon mode should be tunable by simple geometrical modifications of the structure to bring it in resonance with the chosen excitation frequency. In addition to the use of single particle-based antenna structures, coupled particles supporting dimer plasmon modes appear very promising (Kottmann & Martin, 2001; Nordlander *et al.*, 2004). The optical properties of such dimer structures are not only controlled by the particle size,

Correspondence to: A. Christ. Tel: +41 21 693 3968; fax: +41 21 593 2614; e-mail: andre.christ@epfl.ch

they are also strongly influenced by the spatial separation of the individual metal scatterers (i.e. the width of the antenna feed gap).

In this paper we study an alternative approach for the possible realization of surface plasmon tunability. If a metal particle, that is a resonant optical dipole nanoantenna, is placed close to a reflecting metal interface, its plasmonic properties are strongly modified. In addition to the interaction between the individual particle and its own image (Nordlander & Prodan, 2004; Lévêque, 2006), the coupling to delocalized surface plasmon modes on the interface can play a significant role in the response of the system (Cesario *et al.*, 2005; Christ *et al.*, 2006). In particular, we show hat the optical response of such a composite structure depends on the thickness of the underlying metal slab. For the sake of completeness, our theoretical work addresses isolated wires as well as periodic nanowire arrays.

Additionally, the important magnetic properties of the composite structure are briefly discussed. Similar to cut-wire pairs (Dolling *et al.*, 2005), the supported localized plasmon modes of the composite structure can be interpreted in terms of so-called magnetic atoms. Especially, a periodic arrangement of these artificial atoms might be of certain interest. However, although the metamaterial limit is not valid since the elements have dimensions comparable to the wavelength, the magnetic atoms can be arranged to form what is known as magnetic photonic crystal (Linden *et al.*, 2006).

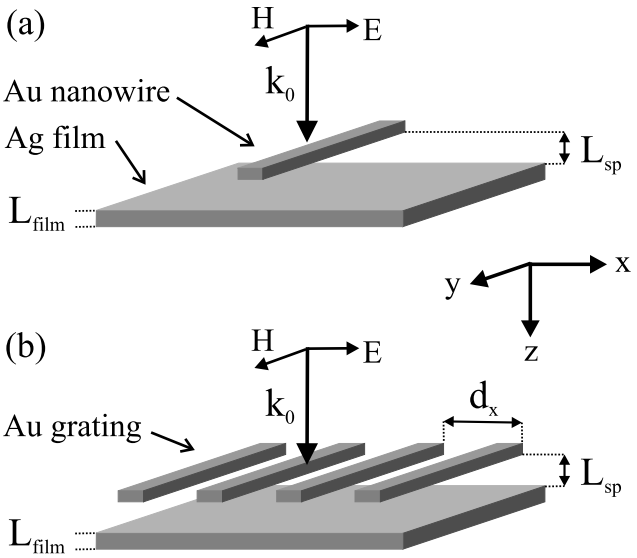

Fig. 1. Schematic view of the two composite metal nanostructures studied in this paper. The structure in panel (a) consits of a single gold nanowire positioned in front of a thin silver slab. The thickness of the metal film L_{film} as well as the wire–slab separation L_{sp} has strong influence on the detected optical response of the system. The other system is shown in panel (b). Instead of a single wire, a periodic nanowire array is considered as the second layer of the composite structure. All studies in this paper are restricted to TM polarization (magnetic field oriented parallel to the nanowires).

Model system and theoretical description

The analyzed composite nanostructures are sketched in panels (a) and (b) of Fig. 1. We consider a two-dimensional nanowire-based geometry. The invariant direction is the *y*-axis, the plane parallel to the silver film is (*Oxy*), and the *z*-axis is oriented normal to the silver interface. Each single gold nanowire is 15 nm thick and 100 nm wide. It is embedded in a fused silica environment of index $n = 1.46$, and is separated from a silver film of thickness L_{film} by a spacer with thickness L_{sp}. The medium below the film (substrate) is fused silica as well. In the case of a nanowire grating, the period is specified by d_x. The incident field is a plane wave that propagates along the *z*-direction. The polarization plane is (*Oxz*) corresponding to transverse magnetic (TM) polarization, that is the magnetic field component of the incident wave is oriented parallel to the metal nanowires.

All calculations for the single-wire case are performed with the dyadic Green's tensor method, based on the solution of the Lippmann–Schwinger equation for the electric field (Martin & Piller, 1998; Paulus *et al.*, 2000; Lévêque *et al.*, 2004). This method is well suited for the study of localized objects embedded in a dielectric and/or metallic multi-layered medium, both for 2D and 3D geometries. Furthermore, a scattering-matrix based formalism has been employed for calculating the optical response of the periodic structure (Tikhodeev *et al.*, 2002). Both methods work without any adjustable fit parameters, and only the geometrical properties and the dielectric susceptibilities of the constituent materials are taken into account as input parameters. Throughout the paper, we use the data of Johnson and Christy for the permittivity of gold and silver (Johnson & Christy, 1972).

Single wire case

We start with the investigation of the single wire case to highlight the modifications of the optical properties induced by the metal film. It has already been shown in Christ *et al.* (2006) and Lévêque & Martin (2006) that the localized plasmon resonance of a metal particle is strongly redshifted when an additional metal film is placed in close proximity. However, the fundamental influence of the metal slab thickness has not yet been investigated. Figure 2 thus displays the numerically obtained intensity of the electric field scattered by a single gold nanowire in dependence of the thickness of the silver slab. The displayed intensities correspond to the field scattered in the incidence medium. In the single-particle spectroscopic studies, the scattered field is computed in the far field, in the direction perpendicular to the interface. The slab thickness is increased from 20 to 50 nm in steps of 5 nm. Additionally, the scattered spectrum of a bare nanowire without the nearby silver film is shown as a reference in both panels.

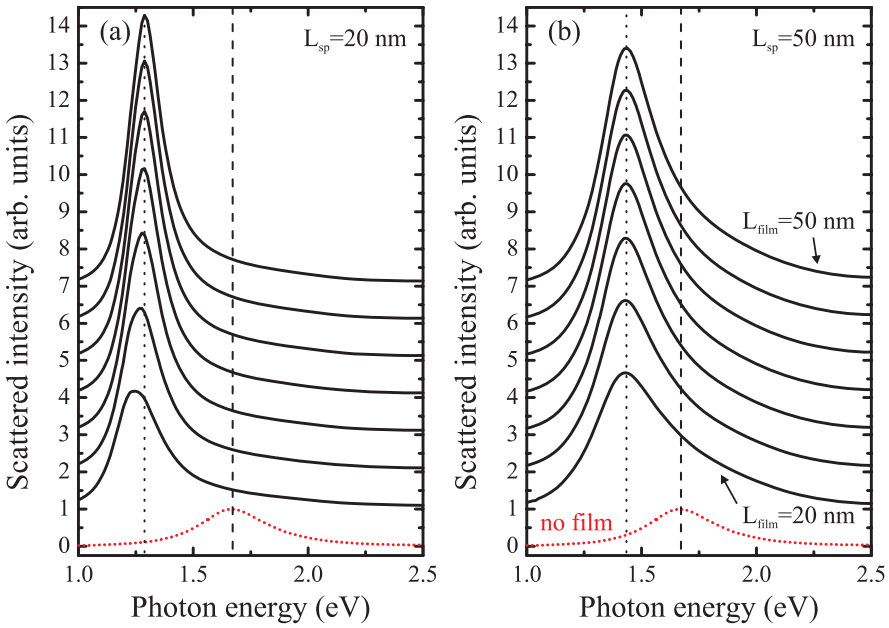

Fig. 2. Intensity of the electric field scattered by an isolated gold nanowire (dotted red lines) and by a gold nanowire placed in front of a silver slab (solid black lines) as a function of the photon energy. Results for structures with wire–film separation of $L_{sp} = 20$ nm (a) and $L_{sp} = 50$ nm (b) are compared for TM polarization. From bottom to top, the slab thickness is increased from $L_{film} = 20$ nm to $L_{film} = 50$ in steps of 5 nm. For clarity, the individual spectra are each shifted upwards by 1 unit.

Wire–film separations of $L_{sp} = 20$ nm, Fig. 2a, and $L_{sp} = 50$ nm, Fig. 2b, are considered. The spectra in Fig. 2 reveal two important phenomena. First, the localized surface plasmon mode of the wire is redshifted from its original position at 1.67 eV due to wire–mirror interaction. The linear restoring forces of the collectively displaced nanowire conduction band electrons are effectively reduced due to near-field coupling with the induced image dipole (which has the opposite orientation). As expected and previously shown, the observed redshift is stronger for smaller spacer thicknesses (Lévêque, 2005). The plasmon related intensity maximum is shifted to 1.28 eV in Fig. 2a and 1.43 eV in Fig. 2b, respectively. Second, the near-field–induced redshift reveals no dependence on the thickness of the nearby silver film. Both panels of Fig. 2 indicate that the observed redshift is only weakly modified when the slab thickness is varied from 20 to 50 nm. This interesting fact is directly related to the small skin depth of the considered silver film (~20 nm); the electromagnetic waves are strongly damped within the first few nanometers of the metal slab. As a result, the observed mirror coupling effect is only weakly modified when the film thickness exceeds the skin depth. By contrast, the achievable scattering intensities are strongly influenced by the thickness of the metal slab. The intensity of the scattered electric field is enhanced with L_{film}, because the silver film reflectivity increases.

Additional information is obtained from the calculated spatial field distributions. Electric (a,c) and magnetic (b,d) field amplitudes in a plane perpendicular to the nanowires are plotted in Fig. 3. An isolated wire and a wire in interaction with the film, assuming a 20-nm-thick silver slab and a 20-nm-thick spacer, are compared. The electric and magnetic fields are shown at the localized plasmon resonance frequencies of 1.67 eV (isolated wire) and 1.24 eV (wire–film), respectively. All fields are normalized to the amplitude of the incident plane wave. Note that the magnetic field is not displayed inside the gold nanowires owing to limitations of the numerical method. Indeed, in the version of the Green's tensor method used for these calculations, the magnetic field is computed by taking the numerical rotational of the electric field. This is possible only outside the object, where the computation step can be arbitrary. On the contrary, the computation step is constant inside the object, and too large for a precise evaluation of the magnetic field.

The field distribution of the localized plasmon mode in the wire–film geometry is characterized by a distinct spatial shape. As schematically indicated in panel (e) of Fig. 3, the related localized resonance can be interpreted in terms of so-called magnetic atoms. Other prominent realizations are the well-known split-ring resonators (Linden *et al.*, 2004) or the closely related cut-wire pairs (Dolling *et al.*, 2005) which have been used as elementary building blocks in recent metamaterial design (Dolling *et al.*, 2006). In particular, the wire–film geometry directly mimics the magnetic, that is the anti-symmetric, dimer plasmon mode of a stacked wire pair. A very simple interpretation is that based on inductor–capacitor (LC) circuits (Meyrath *et al.*, 2006, Unpublished data). The

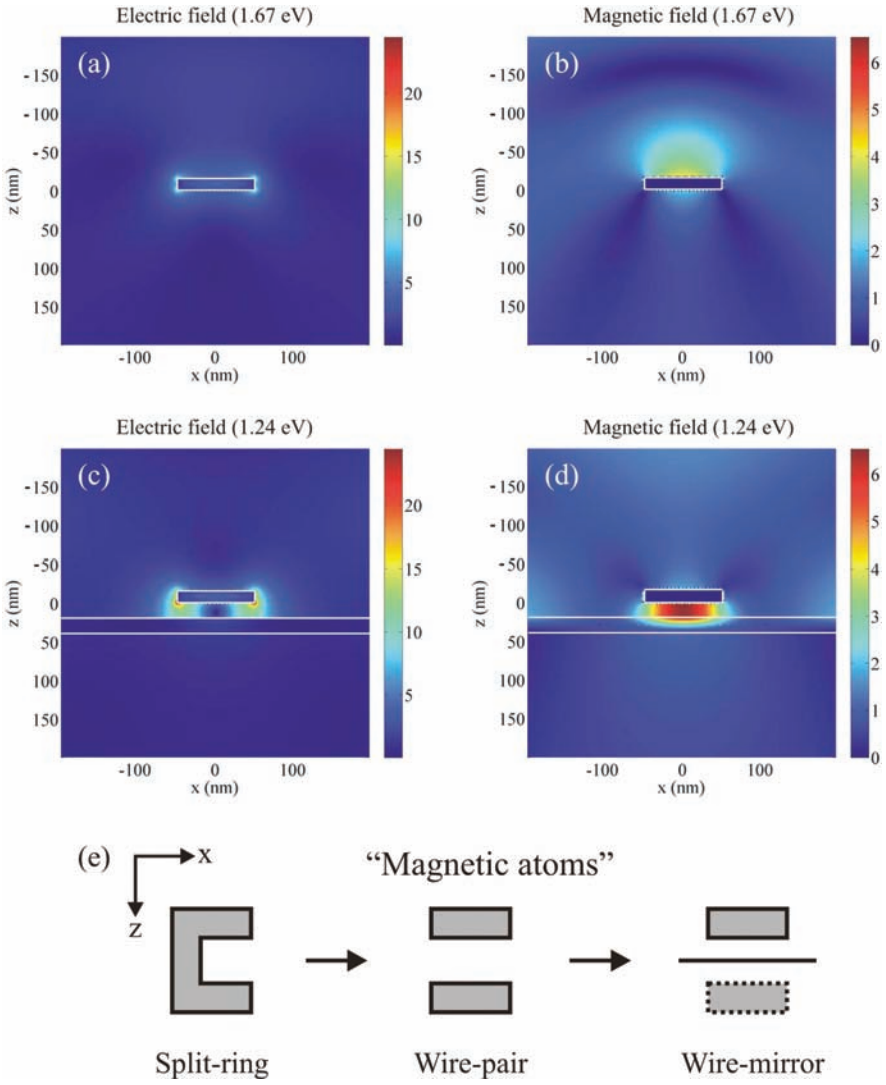

Fig. 3. Distribution of the electric and magnetic field amplitudes for an isolated gold nanowire (a, b) and for a single gold nanowire in front of a 20-nm-thick silver film (c, d). The fields are shown for energies of 1.67 and 1.24 eV in a plane perpendicular to the nanowires. A wire–film separation of $L_{sp} = 20$ nm is chosen in panels (c) and (d). The electric and magnetic fields are normalized to their incident amplitude, respectively. White lines denote the cross-section of the gold wires and the silver film. Owing to the numerical method, magnetic fields are not displayed inside the gold nanowire. Panel (e) illustrates possible realizations of plasmonic resonator geometries: split-ring resonator, wire-pair, and wire-mirror structure.

specific nature of the localized resonance can be directly deduced from the field distributions in panels (c) and (d) of Fig. 3, which indicate that the resonance results from the anti-symmetric coupling of the particle dipole with its image created by the silver layer. This produces a two-lobed structure with high electric fields between the wire edges and the metal slab, indicating the strong displacement currents. The magnetic field in Fig. 3d is mainly concentrated in the spacer below the wire as a result of the induced circular currents. In particular, when the particle is approaching the film, most of the electromagnetic energy is concentrated between the gold particle and the silver film. It has been demonstrated in several studies that the enhancement factor of the electric field between two sharp metallic systems increases for small distances. For example, assuming $L_{sp} = 20$ nm as depicted in panel (c), the enhancement factor of the electric field intensity (at the center between the wire corner and the slab) is about 160 times the incident electric field intensity. The associated enhancement factor of the magnetic-field intensity is around 40 (between the wire and the slab), which is smaller than that associated with the electric field. Without the silver film, as shown in panels (a) and (b), the electric field is mainly concentrated at the corners of the particle. The magnetic field is mainly concentrated on the top of the gold particle, where the incident field constructively interferes with the reflected field.

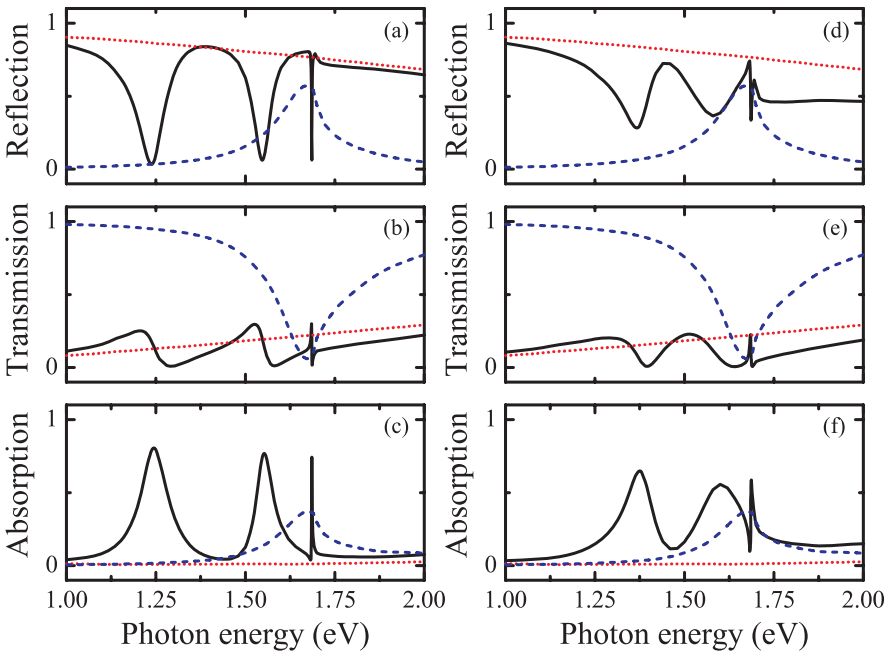

Fig. 4. Calculated reflection, transmission, and absorption spectra for two different surface plasmon polaritonic crystals (solid black lines). The gold gratings with a period of $d_x = 500$ nm are placed in front of a 20-nm-thick silver slab. Structures with a grating–film separation of $L_{sp} = 20$ nm (a–c) and $L_{sp} = 50$ nm (d–f) are considered. The spectra are shown for normal light incidence and TM polarization. Additionally, the spectra of a bare grating (dashed blue lines) and of a bare silver slab (dotted red lines) are shown as reference.

Composite surface plasmon polaritonic crystal

In our next step, we extend the numerical study to composite structures based on periodic nanowire arrays. Therefore the optical properties of so-called surface plasmon polaritonic crystals (see Fig. 1b) are carefully analyzed to clarify the induced spectral changes. In contrast to the discussed single nanowire case, the periodic design now offers an additional degree of freedom. The supported Bloch modes, that is the delocalized surface plasmons of the slab, can be tuned in resonance with the localized mode by changing the geometrical parameters of the structure. The slab thickness as well as the nanowire period have to be controlled to adjust the optical response of the nanostructure.

The nanowire array related modifications are highlighted in Fig. 4 for composite structures with spacer thicknesses $L_{sp} =$ 20 nm (a–c) and $L_{sp} = 50$ nm (d–f). The gold nanowire arrays with a period of $d_x = 500$ nm are placed in front of a 20-nm-thick silver film. The large period is chosen to prevent direct near-field coupling between the individual gold wires of the lattice, which generally results in a redshift of the localized plasmon mode (Rechenberger *et al.*, 2003). Reflection, transmission and absorption spectra are plotted for TM polarization and normal incidence. Figure 4 also includes the numerical spectra of two reference structures. First, the spectra of the bare grating without metal film are shown (dashed blue line). Second, the spectra of an unstructured 20-nm-thick silver film are included (dotted red lines). Generally, two types of surface plasmon polariton modes should be supported by the nanowire-array–based composite structure. In addition to localized wire plasmon modes, the Bragg-periodic nature should allow for efficient excitation of delocalized surface plasmon modes at the nearby silver film. If the metal grating is considered as a weak perturbation, the silver slab is characterized by a symmetric surrounding (i.e. the metal slab is coated by silica on both sides). As a result, the surface plasmon modes at both interfaces of the thin film couple. The degeneracy is lifted, and short- and long-range modes are formed (Burke *et al.*, 1986). It should be mentioned that the single wire geometry also generally allows for excitation of delocalized surface plasmon modes (Ditlbacher *et al.*, 2002). However, in comparison to the localized plasmon mode, the excitation efficiency of delocalized modes is much weaker.

As a matter of fact, the spectra in Figs 4a–c give direct evidence for the excitation of various surface plasmon modes. Instead of a single spectral feature (e.g. see Fig. 2), three pronounced resonances can be observed. The three pronounced absorption maxima are related to reflection minima and dispersive (Fano-like) features in the transmission spectra. Two spectrally broad modes are accompanied by a single narrow line. The reference spectra by contrast show no surprising results. For example, the spectra of the silver films (dotted red lines in Fig. 4) are more or less

structureless whereas the localized wire plasmon of the bare grating can be directly observed (dashed blue lines in Fig. 4).

The nature of the different resonances observed in Fig. 4 can be easily deduced from the corresponding field distributions. The numerically obtained spatial distributions of the electric and magnetic fields are therefore displayed in Fig. 5 for normal light incidence and TM polarization. Shown are the normalized time-averaged field amplitudes for a nanowire structure with a period of $d_x = 500$ nm, an array–film separation of $L_{sp} = 20$ nm, and a 20-nm-thick silver film. The local fields are plotted for incoming photon energies of 1.245, 1.553 and 1.685 eV. The chosen photon energies correspond to the spectral positions of the absorption maxima in Fig. 4c.

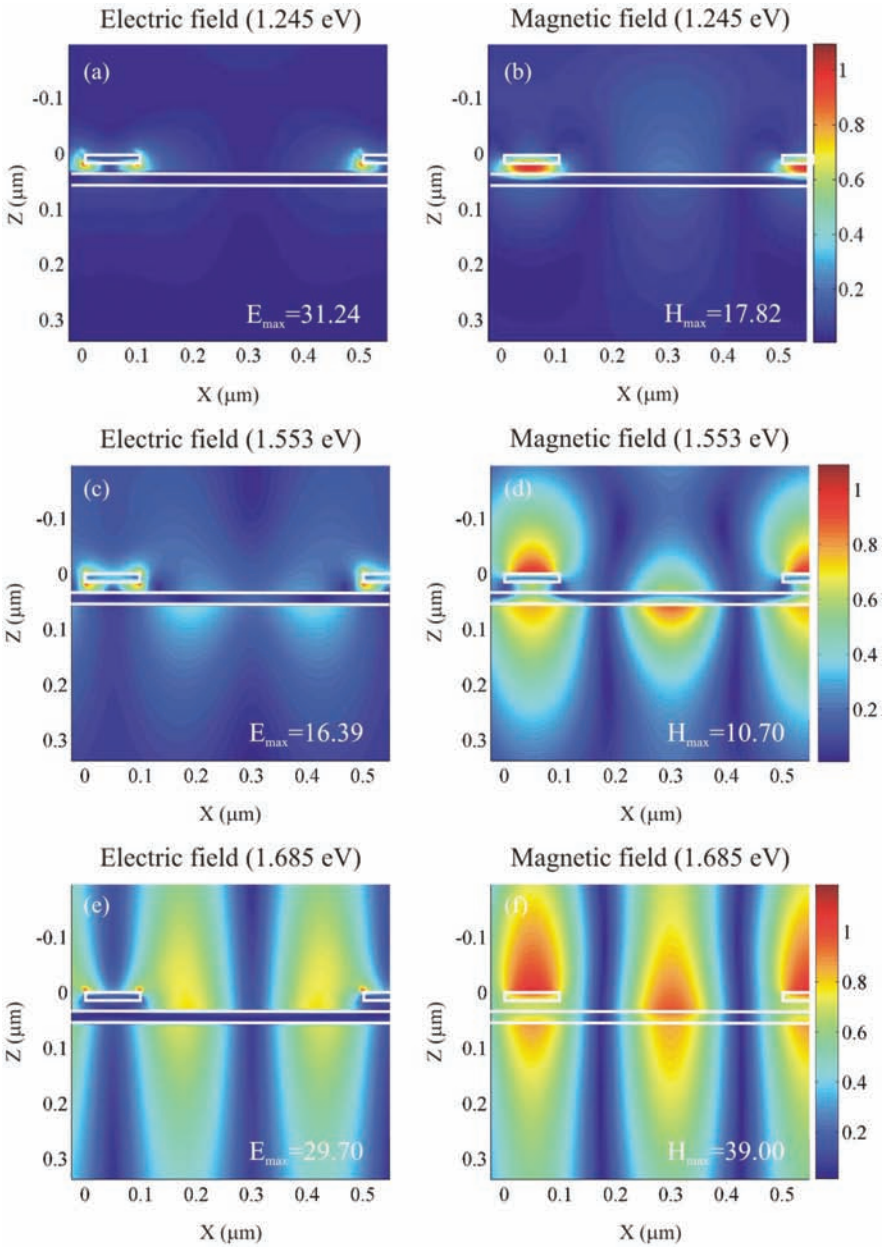

Fig. 5. Calculated spatial field distributions of the electric and magnetic fields for normal light incidence and TM polarization. Shown are the normalized time-averaged field amplitudes for a nanowire structure with a periodicity of $d_x = 500$ nm, a grating–film separation of $L_{sp} = 20$ nm and a 20-nm-thick silver slab. The local fields are depicted for an incoming photon energy of $\hbar\omega = 1.245$ eV (a, b), $\hbar\omega = 1.553$ eV (c, d) and $\hbar\omega = 1.685$ eV (e, f) in a plane perpendicular to the nanowires. The chosen energies correspond to the positions of the absorption maxima in Fig. 4c. The field distributions are normalized to the maximum electric or magnetic field (value is indicated in each panel) measured in units of the incoming field with amplitudes equal to one. White lines indicate the cross-section of the gold wires and the silver film.

The first maximum at 1.245 eV can be directly attributed to the excitation of a localized plasmon mode. Its energy approximately fits the spectral position of the surface plasmon mode of the single wire-based composite structure in Fig. 2a. Furthermore, the corresponding fields show the identical characteristic spatial distribution already discussed for the single wire case in Figs 3c and d. Strong electric fields are found at both edges of the gold nanowires. The magnetic field by contrast is concentrated directly below the wires, that is within the 20-nm-thick spacer. Similar to the single wire case, the individual nanowires of the ensemble act as small dipole antennas and induce image dipoles within the metal film. Near-field coupling leads to a modification of the effective linear restoring forces that arise due to the collectively displaced nanowire conduction band electrons. As a result, the supported localized plasmon mode is strongly redshifted in comparison to the sole resonance of the bare grating (dashed lines in Fig. 4). Note that the periodic arrangement of individual magnetic atoms can be interpreted in terms of a so-called one-dimensional magnetic photonic crystal (Linden *et al.*, 2006).

The character of the second resonance at 1.553 eV in Fig. 4c differs from the localized surface plasmon mode. The corresponding field distributions in panels (c) and (d) of Fig. 5 reveal evanescent field components on both sides of the metal slab. Furthermore, the strong fields are not only localized near the individual wires. For example, an additional maximum of the magnetic field can be found in between two adjacent nanowires. Thus, the resonance can be undoubtedly identified as a grating-induced surface plasmon mode of the metal slab. An additional grating-induced surface plasmon mode can be found at 1.685 eV, that is at the spectral position of the narrow absorption line in Fig. 4c. The corresponding field distributions in panels (e) and (f) of Fig. 5 show a very similar structure as the fields of the lower energy surface plasmon mode. However, the decay lengths of the evanescent electric and magnetic field components into the ambient silica half spaces are much longer now.

The correctness of the interpretation can be further checked by analytically calculating the dispersion of the supported surface plasmon modes (Burke *et al.*, 1986). In contrast to single nanowire-based structures, where surface plasmons with various propagation vectors k_x can be excited at the nearby metal slab, a periodic wire arrangement restricts the possible plasmon excitation to surface modes with specific in-plane momenta. The dispersion of the short- and long-range surface plasmon modes of a 20-nm-thick silver slab (embedded in silica) are therefore shown in panel (a) of Fig. 6 in empty lattice approximation. In this approximation, the mode dispersion is calculated assuming a bare metal layer neglecting the nearby nanowire array. The branches of the dispersion curves are then folded into the first Brillouin zone, assuming a periodicity of $d_x = 500$ nm. The extracted spectral position of the long-range surface plasmon at 1.684 eV (crossing point of the branches at the center of Brillouin zone) corresponds very well with the energy of the sharp absorption maximum at

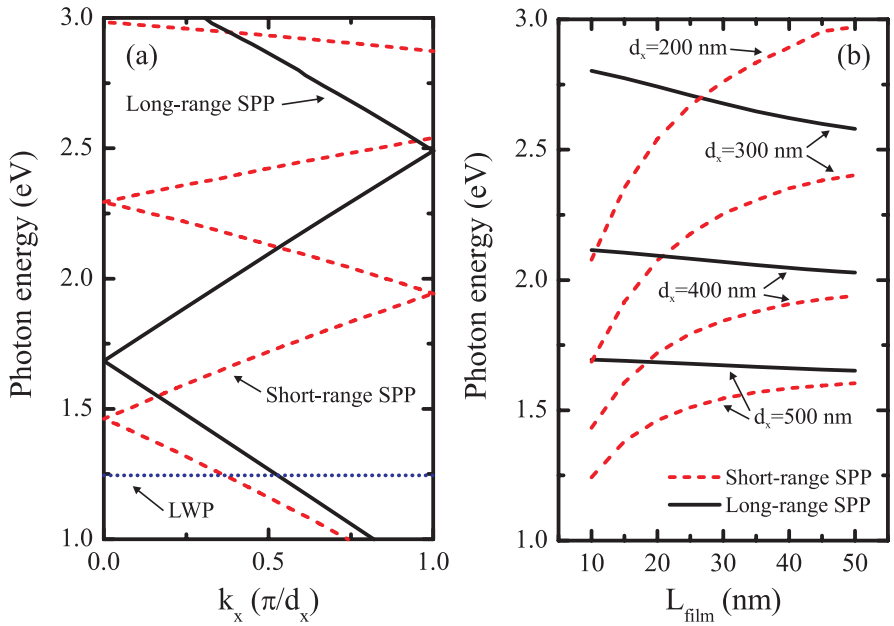

Fig. 6. (a) Dispersion of the short- (dashed red lines) and long-range (solid black lines) surface plasmon modes of a 20-nm-thick silver film in empty-lattice approximation. The modes are folded into the first Brillouin zone assuming a periodicity of $d_x = 500$ nm. Additionally, the position of the localized wire plasmon (LWP) is plotted for a spacer thickness of $L_{sp} = 20$ nm. (b) Spectral position of the short- and long-range surface plasmon modes in dependence of the silver film thickness L_{film}. Periods of $d_x = 200$ nm, $d_x = 300$ nm, $d_x = 400$ nm and $d_x = 500$ nm are considered.

1.685 eV in Fig. 4c. The large propagation length, that is the long lifetime of this surface plasmon mode, is reflected by the narrow spectral linewidth and the related field distribution. As already shown in panel (e) of Fig. 5, the electric field is mainly concentrated outside of the metal slab, indicating low absorption losses. The short-range mode can be found at 1.461 eV in empty lattice approximation, which is very close to the spectral position of the second maximum at 1.553 eV in Fig. 4c. The short-range character of the mode is reflected by the broadening of the absorption line. The observed spectral shift can be simply explained by the coupling with the nearby localized plasmon at 1.245 eV which results in a small blueshift in comparison to the analytical solution. This coupling effect also influences the corresponding field distribution. As shown in panels (c) and (d) of Fig. 5, the field distribution has a clear grating-induced surface plasmon character. However, the electric field has already strong components around the individual nanowires, indicating the onset of mode mixing between localized and delocalized resonances.

The important modification due to coupling between localized and delocalized modes is further highlighted in panels (d), (e), and (f) of Fig. 4. The gold grating with a period of $d_x = 500$ nm is again placed in front of a 20-nm-thick silver film. However, the spacer thickness is now increased from $L_{sp} =$ 20 nm to $L_{sp} = 50$ nm. For example, the absorption spectrum in panel (f) is strongly modified in comparison to the results in panel (c). The thicker spacer weakens the influence of the mirror coupling effect, which results in a reduced redshift of the localized surface plasmon mode. Considering the previous results of Fig. 2, the localized surface plasmon should be found at 1.43 eV. This energy is in close resonance with the position of the bare short-range surface plasmon mode at 1.46 eV. The interaction between both modes leads to a spectral splitting (i.e. lifting of the degeneracy) owing to polariton formation. Although one peak is lowered in energy to 1.37 eV, the second peak is blueshifted and interferes with the spectrally narrow long-range surface plasmon mode at 1.685 eV.

Finally, we study the influence of the metal film thickness on the optical properties of the composite structure. As already discussed in the previous section, the nanowire–film interaction (i.e. image coupling) is only weakly modified when changing the metal slab thickness from 20 to 50 nm. However, the coupling between localized and delocalized modes should be strongly affected by the changed surface plasmon dispersion. The analytically obtained spectral positions of the short- and long-range surface plasmon modes of a thin silver film are depicted in Fig. 6b in dependence of the slab thickness L_{film}. The dispersion curves, extracted from an empty lattice approximation, are shown for periods of 200, 300, 400, and 500 nm. Generally, a stronger coupling between the bare surface plasmon modes at both slab–silica interfaces for gradually decreasing film thicknesses results in a larger energy splitting between the arising short- and long-range plasmon modes. A variation of the Brillouin zone size additionally modifies the spectral dependence. A larger period, that is a smaller Brillouin zone shifts the resonances to lower energies. The dispersions of both surface plasmon modes approach the quartz light line in this spectral regime and a smaller mode splitting can be observed.

The related scattering matrix–based results are displayed in Fig. 7 to highlight the L_{film} dependence of the composite structure. Extinction spectra for TM polarization and normal light incidence are shown for structures with wire periods of 200 nm (a), 300 nm (b), 400 nm (c), and 500 nm (d). Although the spacer thickness of $L_{sp} = 50$ nm is kept constant, the slab thickness L_{film} is increased from 0 to 50 nm in steps of 10 nm. A thicker spacer of $L_{sp} = 50$ nm (instead of $L_{sp} =$ 20 nm) has been chosen to weaken the image coupling and hence reduce the redshift of the localized suface plasmon. As a result, the localized mode is shifted to higher energies and hence in resonance with the slab plasmon modes.

The depicted dependencies reveal several characteristic features. Similar to the single wire structures, the localized plasmon mode is redshifted due to wire–film interaction. It is important to note that the localized resonance is characterized by an asymmetric, that is Fano-type line shape. The composite structure acts as a metal microcavity (Hibbins *et al.*, 2006) and the interference between direct and resonance-assisted transmission channels has to be taken into account. For example, the upper spectrum in panel (a) of Fig. 7 reveals a strong extinction maximum at 1.69 eV that is accompanied by an accentuated minimum at 1.24 eV. The related absorption maximum at approximately 1.43 eV (not shown) however corresponds very well to the single wire value extracted from Fig. 2b. In other words, the spectral position of the localized surface plasmon mode is slightly redshifted in comparison to the observed extinction maximum.

More dramatic effects are related to the direct coupling between the supported surface plasmon modes. For a nanowire period of $d_x = 200$ nm, localized and delocalized modes are more or less spectrally separated. A pronounced spectral feature that is related to the short-range surface plasmon mode can only be observed at 2.1 eV for $L_{film} = 10$ nm. For larger slab thicknesses, the short-range mode is blueshifted and appears as a weakly pronounced dip in the spectra. The situation changes dramatically when the period is increased, that is the thickness-dependent dispersion of the delocalized surface plasmon modes is shifted to lower energies. For example, panel (d) of Fig. 7 indicates a strong interaction due to the spectral overlap of the supported bare plasmon modes. A clear anti-crossing between the localized and the delocalized short-range surface plasmon resonances can be observed. The short-range mode is found energetically below the localized plasmon in case of $L_{film} =$ 10 nm. The resonance shows up as a narrow peak at 1.19 eV. As explained previously, the mode is blueshifted when increasing the silver slab thickness. The mode approaches the spectral position of the long-range surface plasmon that is already

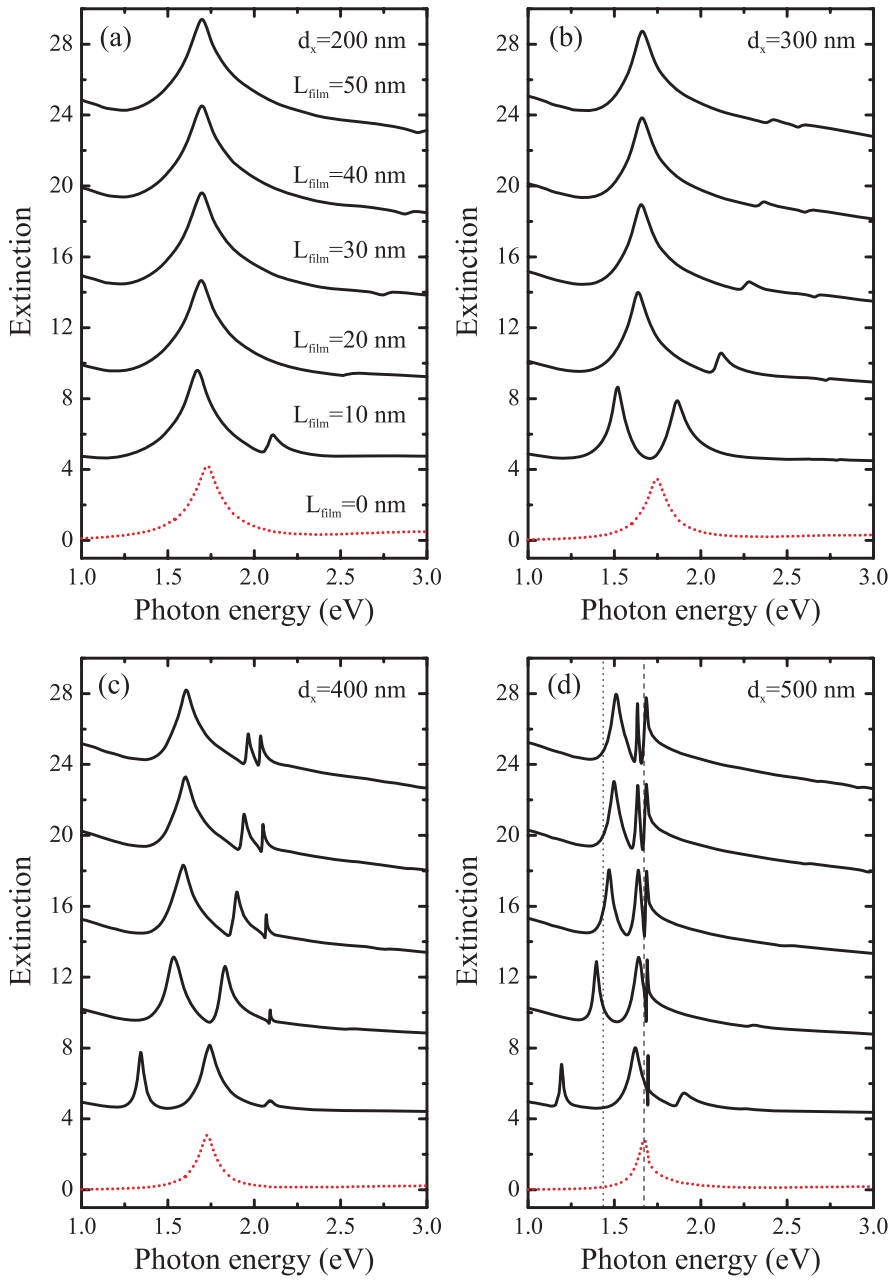

Fig. 7. Calculated extinction spectra for surface plasmon polaritonic crystals. The spectra are shown for normal light incidence and TM polarization. Structures with grating periods of $d_x = 200$ nm (a), $d_x = 300$ nm (b), $d_x = 400$ nm (c) and $d_x = 500$ nm (d) are studied. The spacer thickness $L_{sp} = 50$ nm is kept constant. From bottom to top, the silver slab thickness is increased from $L_{film} = 0$ nm to $L_{film} = 50$ nm in steps of 10 nm. The spectra of the bare gratings are indicated by the red dotted lines. For clarity, the individual spectra are each shifted upwards by 4 units. The vertical lines in panel (d) indicate the energies of the localized plasmon in case of the single wire structure: bare wire (dashed line) and wire–film geometry (dotted line).

tuned into resonance with the localized plasmon. For $L_{film} = 50$ nm, a direct mixing between three plasmon resonances can be observed.

It might be very interesting to study the non-linear properties of these magnetic photonic crystals in future experiments. For example, similar to Mühlschlegel *et al.* (2005), the achievable high electromagnetic field intensities should allow for white-light supercontinuum generation. In particular, the slab thickness provides an additional geometrical tuning parameter to influence the light–matter interaction. Especially the impact of the discussed polariton formation on the non-linear properties should be clarified.

Conclusion

In conclusion, we have analyzed the tunability of surface plasmon polariton modes in composite metallic nanostructures. The optical spectra of two simple model systems have been compared to distinguish between effects that are either related to the individual nanowires or to the collective response of a periodic nanowire ensemble. As expected, the wire–film interaction results in a near-field induced redshift of the localized wire plasmon resonance. However, although the effect is characterized by a strong dependence on the spacer thickness, the redshift of the localized mode is only weakly influenced by a thickness variation of the metal slab. The situation changes if a periodic nanowire arrangement is applied. Now the interaction between localized wire plasmons and grating-induced surface plasmons of the metal slab results in further spectral modifications. The plasmon–plasmon interaction can be directly controlled by changing the metal film thickness, that is by changing the dispersion of the delocalized short- and long-range surface plasmon modes. Generally, the presented effects reveal fundamental plasmonic functionalities that are important with regard to the design of plasmon-based nanodevices.

Acknowledgements

We acknowledge financial support by the European Commission (FP6-2002-IST-1-507879), the German Federal Ministry of Education and Research (FKZ 13N8340/1), the Deutsche Forschungsgemeinschaft (SPP1113, FOR557), the Russian Academy of Science, and the Russian Foundation for Basic Research (06-02-17211).

References

Burke, J.J., Stegeman, G.I. & Tamir, T. (1986) Surface-polariton-like waves guided by thin, lossy metal films. *Phys. Rev. B* **33**, 5186.

Cesario, J., Quidant, R., Badenes, G. & Enoch, S. (2005) Electromagnetic coupling between a metal nanoparticle grating and a metallic surface. *Opt. Lett.* **30**, 3404.

Christ, A., Zentgraf, T., Tikhodeev, S.G., Gippius, N.A., Kuhl, J. & Giessen, H. (2006) Controlling the interaction between localized and delocalized surface plasmon modes: experiment and numerical calculation. *Phys. Rev. B* **74**, 155435.

Ditlbacher, H., Krenn, J.R., Felidj, N., *et al.* (2002) Fluorescence imaging of surface plasmon fields. *Appl. Phys. Lett.* **80**, 404.

Dolling, G., Enkrich, C., Wegener, M., Soukoulis, C.M. & Linden, S. (2006) Simultaneously negative phase and group velocity of light in a metamaterial. *Science* **312**, 892.

Dolling, G., Enkrich, C., Wegener, M., Zhou, J.F., Soukoulis, C.M. & Linden, S. (2005) Cut-wire pairs and plate pairs as magnetic atoms for optical metamaterials. *Opt. Lett.* **30**, 3198.

Hibbins, A.P., Murray, W.A., Tyler, J., Wedge, S., Barnes, W.L. & Sambles, J.R. (2006) Resonant absorption of electromagnetic fields by surface plasmons buried in a multilayered plasmonic nanostructure. *Phys. Rev. B* **74**, 073408.

Homola, J., Yee, S.S. & Gauglitz, G. (1999) Surface plasmon resonance sensors: review. *Sens. Actuators* **54**, 3.

Johnson, P.B. & Christy, R.W. (1972) Optical constants of the noble metals. *Phys. Rev. B* **6**, 4370.

Kottmann, J.P. & Martin, O.J.F. (2001) Plasmon resonant coupling in metallic nanowires. *Opt. Express* **8**, 655.

Kottmann, J.P., Martin, O.J.F., Smith, D.R. & Schultz, S. (2001) Plasmon resonances of silver nanowires with a nonregular cross section. *Phys. Rev. B* **64**, 235402.

Lévêque, G. & Martin, O.J.F. (2006) Tunable composite nanoparticle for plasmonics. *Opt. Lett.* **31**, 2750.

Lévêque, G., Mathevet, R., Weiner, J., *et al.* (2004) Modelling resonant coupling between microring resonators addressed by optical evanescent waves. *Nanotechnology* **15**, 1200.

Linden, S., Decker, M. & Wegener, M. (2006) Model system for a one-dimensional magnetic photonic crystal. *Phys. Rev. Lett.* **97**, 083902.

Linden, S., Enkrich, C., Wegener, M., Zhou, J., Koschny, T. & Soukoulis, C.M. (2004) Magnetic response of metamaterials at 100 terahertz. *Science* **306**, 1351.

Maier, S.A., Brongersma, M.L., Kik, P.G. & Atwater, H.A. (2002) Observation of near-field coupling in metal nanoparticle chains using far-field polarization spectroscopy. *Phys. Rev. B.* **65**, 193408.

Martin, O.J.F. & Piller, N.B. (1998) Electromagnetic scattering in polarizable backgrounds. *Phys. Rev. E* **58**, 3909.

Moskovits, M. (1985) Surface-enhanced spectroscopy. *Rev. Mod. Phys.* **57**, 783.

Mühlschlegel, P., Eisler, H.J., Martin, O.J.F., Hecht, B. & Pohl, D.W. (2005) Resonant optical antennas. *Science* **308**, 1607.

Nordlander, P., Oubre, C., Prodan, E., Li, K. & Stockman, M.I. (2004) Plasmon hybridization in nanoparticle dimers. *Nano Lett.* **4**, 899.

Nordlander, P. & Prodan, E. (2004) Plasmon hybridization in nanoparticles near metal surfaces. *Nano Lett.* **4**, 2209.

Paulus, M., Gay-Balmaz, P. & Martin, O.J.F. (2000) Accurate and efficient computation of the Green's tensor for stratified media. *Phys. Rev. E* **62**, 5797.

Rechenberger, W., Hohenau, A., Leitner, A., Krenn, J.R., Lamprecht, B. & Aussenegg, F.R. (2003) Optical properties of two interacting gold nanoparticles. *Opt. Commun.* **220**, 137.

Rockstuhl, C., Lederer, F., Etrich, C., Zentgraf, T., Kuhl, J. & Giessen, H. (2006) On the reinterpretation of resonances in split-ring-resonators at normal incidence. *Opt. Express* **14**, 8827.

Tikhodeev, S.G., Yablonskii, A.L., Muljarov, E.A., Gippius, N.A. & Ishihara, T. (2002) Quasi-guided modes and optical properties of photonic crystal slabs. *Phys. Rev. B* **66**, 045102.